Applied Physics A (2025) 131:37
https://doi.org/10.1007/s00339-024-08122-1

Synchrotron-based diffraction-enhanced imaging and diffraction-enhanced imaging combined with CT X-ray imaging systems to image seeds at 30 keV

D. V. Rao[1] · G. E. Gigante[1] · Z. Zhong[2] · R. Cesareo[3] · A. Brunetti[3] · N. Schiavon[4] · T. Akatsuka[5] · T. Yuasa[5] · T. Takeda[6]

Received: 17 June 2024 / Accepted: 22 November 2024 / Published online: 18 December 2024

Abstract
Utilized the upgraded Synchrotron-based non-destructive Diffraction-enhanced imaging and Diffraction-enhanced imaging coupled with CT X-ray imaging systems to image the chickpea seeds, to enhance the contrast in plant root architecture, visibility of fine structures of root architecture growth and some aspects of physiology at acceptable level. DEI-CT images were acquired with 30 keV synchrotron X-rays. A series of DEI-CT slices were assembled together, to form a 3D data set. DEI-CT images explored more structural information and morphology. Noticed detailed anatomical, physiological observations, and contrast mechanisms. With these systems, some of the complex plant traits, root morphology, growth of laterals and subsequent laterals can be visualized directly.

Keywords Synchrotron X-rays · DEI · DEI-CT · Chick pea · Seeds · Imaging · Physiology · Contrast

1 Introduction

Synchrotron-based techniques have been increasingly employed in various fields of physical, chemical, biological, geological, medical, material, and life sciences. Images from the samples demonstrate very weak absorption contrast, nevertheless producing significant phase shifts in the X-ray beam. Image processing derives structural features, which are then numerically quantified by image analysis. Contrast enhancement plays an important role in image processing; it enhances structural features that are hardly detectable to the human eye and allows automatic extraction of those features. Extended, X-ray phase-contrast and also tomography mode applications in various fields are available with synchrotron-based systems [1–8]. Further, observation of unstained small seed using laboratory-based X-ray phase-contrast CT is introduced [9]. The implementation of phase contrast based Sy-DEI and Sy-DEI-CT enables the investigation of the connectivity of the interior structure, which are invisible to the absorption contrast, while are readily observed in phase contrast [10–11]. These imaging techniques are useful tools to examine the plant anatomy and physiology. Interaction between the light and plant, takes place, through reflected, absorbed or transmitted photons. Tomographic imaging with X-ray photons has been used in the non-destructive study of plant-soil interactions for a number of years. However, these techniques are very limited in use in the field of agriculture [12–27], and food and measurement [28–29]. With CT system, a series of 2D images, from an object can be scanned, in a single axis of rotation and an assembly of 2D images, generates 3D image of an object. 3D volumetric data, from the growth of laterals and the subsequent laterals, provide the interior plant

✉ D. V. Rao
done9venkat53@rediffmail.com

1 Department of Science Based Applications to Engineering (SBAI), Physics Division, University of Rome "La Sapienza", Via Scarpa 10, Roma 00161, Italy

2 Brookhaven National Laboratory, National Synchrotron Light Source, Upton, NY, USA

3 Istituto di Matematica e Fisica, Università di Sassari, Via Vienna 2, Sassari 07100, Italy

4 Hercules Laboratory, University of Evora, Evora, Portugal

5 Department of Bio-System Engineering, Faculty of Engineering, Yamagata University, Yonezawa- shi, Yamagata 992-8510, Japan

6 Allied Health Science, Kitasato University, 1-15-1 Kitasato, Sagamihara, Kanagawa 228-8555, Japan

structures and root architecture. As regards to image analysis, ninety-two, different image analysis software tools are available, to study the plant biology (http://www.plant-image-analysis.org).

In recent years, improvements in image quality were carried out regularly on phantoms and biological samples with SY-DEI and SY-DEI-CT systems. Based on above and in continuation of our research, we have chosen Sy- DEI and Sy-DEI-CT systems to image seeds and their growth at different intervals of time. Limited studies have been reported using high energy X-ray imaging systems with synchrotron radiation, for imaging and quantifying plant root systems in situ [30–31]. A need therefore exists to evaluate these higher energy tomographic imaging systems with regards to resolution, noise and contrast. Since plant roots have higher water content, we hypothesize that, synchrotron-based systems are excellent tools for the observation and quantification of fine plant roots in situ. Plant roots serve as important organs for water and nutrient uptake, synthesis of growth regulators and storage of carbohydrates. In this investigation, we report on the potential use of the synchrotron-based imaging systems to study the nature of plant roots at a spatial resolution of about 9 μm or larger. On the other hand, non-destructive analysis is of great interest to a broad community of potential users in the field of agriculture and biological sciences [32].

Earlier researchers studied the plants by non-invasive image analysis [33], plant growth [34], mesh processing based technique for 3D plant analysis [11], and maize roots [35]. Further, various approaches, such as, 3D analysis of plant structure using X-ray CT [36], measuring root traits acquisition [37], analysis of CT scan data non-destructive visualization [38], quantification of root using CT [39] and visualization of undisturbed root architecture [40–41], were examined extensively. The spatial resolution of the present systems was 9 μm and has the potential of enabling entire root systems of seedlings are to be reconstructed. Further, research has been planned to examine the growth rate, track development in growth plant with anatomical mutations and imaging the root growing in opaque matrix.

2 Experimental details

2.1 The DEI system

The details of diffraction-enhanced imaging technology and the associated instrumentation have been presented previously [42–44] and we will high-light the X-ray optics scheme, with a brief description here. Figure 1 shows the schematic of the DEI system used for our experiments available at the X-15 A beamline, at NSLS, BNL, USA and for DEI-CT, the sample is placed on a Huber (Blake Industries, Scotch Plains, NJ) rotational stage. Highly collimated beam of X-rays are prepared by the Silicon [3] monochromator consisting of two perfect silicon crystals. Once this beam passes through the sample, a third crystal (analyzer crystal) of the same reflection index diffracts the X-rays onto radiographic film (Kodak Professional Industrie 150, Industrex SR45), an image plate detector (Fuji HRV image plate, read out by a Fuji BAS2500 image plate reader at 50 micron pixel size) or a X-ray CCD detector (Photonic Science VHR camera, 9 micron pixel size).

2.2 Samples

ChickPnP Kabuli Chana, and a variety of other types are available at local grocery store (Fig. 2 (a)). We have chosen, ChickPnP Kabuli Chana, for the present study. Management practices are followed to grow the crop, to protect the crop from any insects and to avoid routine moisture. This way, the profile structure is maintained, throughout the study. Figure 2 (b) shows the growth rate after twenty four hours. Chickpea seed samples were washed for surface-sterilization in a weak solution of 10% sodium hypochlorite. The distribution of water to seeds is varied from 24 h to 240 h. Dry seed and a germinated seed were selected during the above time period. The germination process is imaged every day, and continued up to few days. Figure 3 shows the dependence of phase to attenuation contrast ratio (δ / β), for few soft biological samples suitable for the present study. δ and β vary with the sample electronic density and the incident photons energy E (in 1/E for β in the X-ray range of energy and $1/E^3$ for δ). Increasing the energy in the X-ray beam will reduce the total change in angle and will increase the slope of the reflectivity profile. As a result, DEI contrast only decreases as 1/E; doubling the energy of the X-ray beam only results in a two-fold decrease in image contrast. Figure 4 Shows the root architecture laterals, subsequent laterals, and their lengths, growth of the seed before the acquisition of the images and the roots used for DEI-CT image reconstruction. The length of the root varies from 2 to 5 cm and the diameter varies approximately from 1.5 mm to 2 mm. DEI images in planar mode are acceptable visibility compared to conventional X-ray images, because higher energy X-rays (30 keV) are used and refracted X-rays are measured as data. An additional advantage of using high-energy X-rays is that the absorbed radiation dose is low. The amount of radiation absorption has been calculated to be approximately 0.12 mGy per exposure. It will not affect germination or growth significantly. For the 2D scan, the dose differs with CT scan, with an amount of 1–2%.

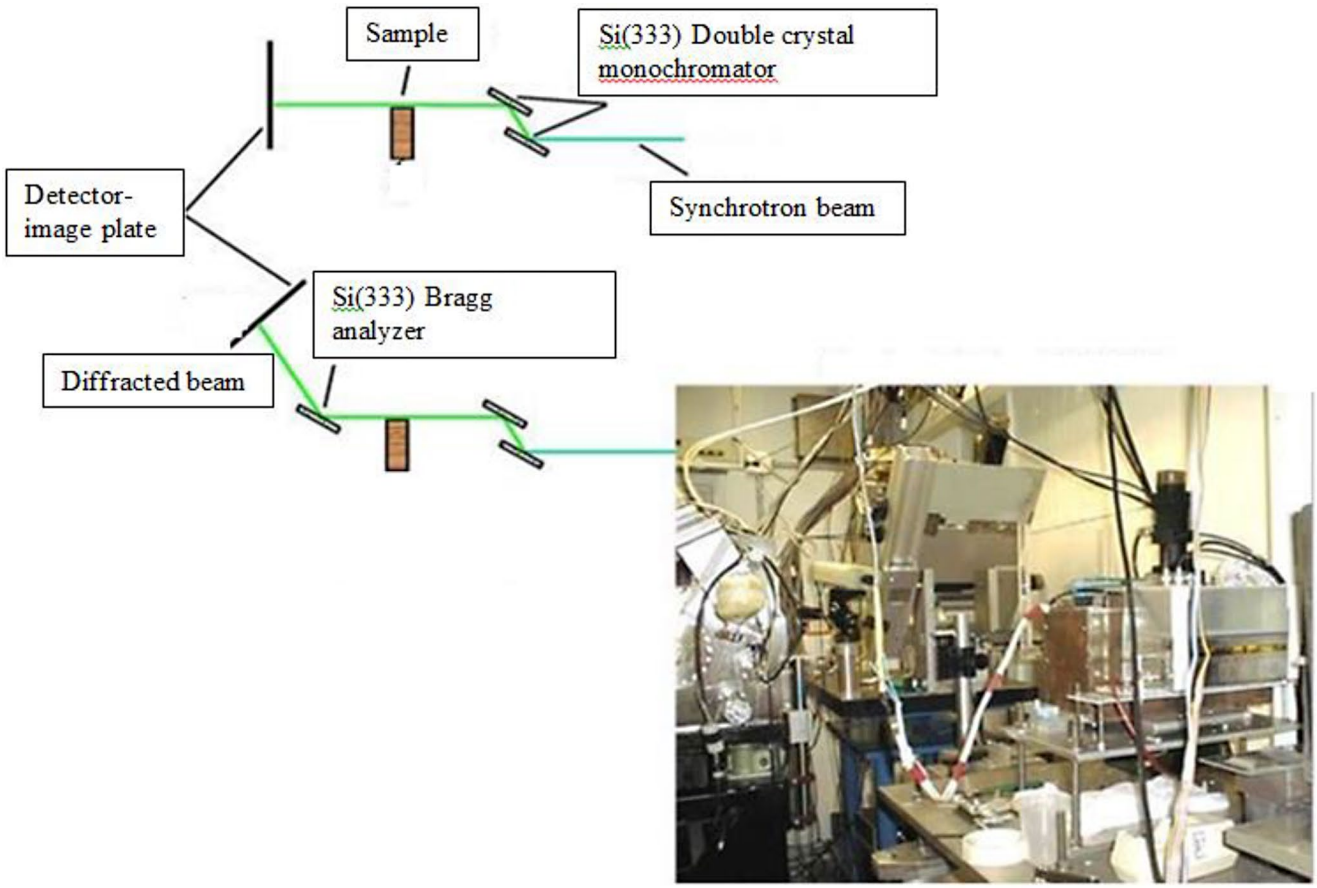

Fig. 1 Experimental Sy-DEI and Sy-DEI-CT systems available at X-15 A, NSLS, BNL, USA. X-rays are analyzed in angle using perfect silicon crystal, after passing through the sample

Fig. 2 (**a**) ChickPnP Kabuli Chana, available at local grocery store (**b**) Chick pea seeds of different dimensions and growth after 24 h

(a) (b)

2.3 Data analysis

For the planar mode Sy-DEI imaging, the sample stage scanned the sample vertically through the X-ray beam. These images were processed using the background subtraction tool in Image Pro Express 5.1 (Media Cybernetics, Bethesda, MD) and acquired 21images at different analyzer positions for each sample. Sy-DEI-CT scans were performed for the sample by fixing the analyzer crystal at a specific angle and rotating the sample stepwise through 360^0 at 0.5^0 or 0.18^0 increments. The specific angle for the analyzer crystal was fixed at 11.62^0. For each image in CT mode, 720 or 2,000 projections were acquired with a sample rotation step size of 0.5^0 or 0.18^0, and with an acquisition time of 1s per image. For tomographic reconstruction, a filtered back projection algorithm was used. Custom programs written in Interactive Data Language (IDL) were used to perform all of the image analysis, tomographic reconstructions and graphic visualization. The resolution of the detector is 9 μm but the reconstruction was performed with 2×2 rebining to achieve a voxel size of 18 microns.

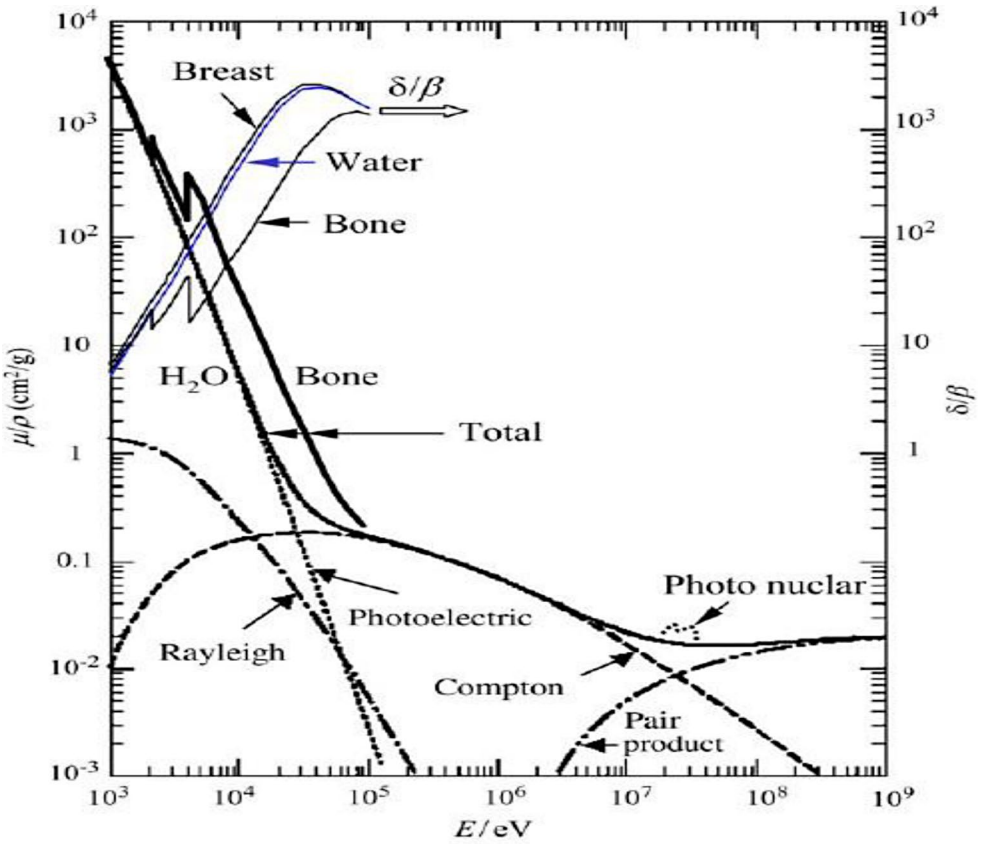

Fig. 3 The dependence of phase to attenuation contrast ratio (δ / β), for few soft biological samples suitable for the present study [44]

Fig. 4 Sample and preparation for acquisition for experiments and for installation on rotation stage of the x-ray system. The root laterals, subsequent laterals, and their lengths, growth of the seed before the acquisition of the images and the roots used for CT image reconstruction. Seeds, after watering for 24 h to 240 h. The length of the root varies from 2 to 5 cm and the diameter varies approximately from 1.5 mm to 2 mm

Beamline control and data collection were handled by a program called spec (Certified Scientific Software, Cambridge, MA, USA). The data was subsequently manipulated and images displayed using Igor Pro.5.04 (Wavemetrics, Lake Oswego, OR, USA). Each vertical column of image data was normalized, using a region of the image that did not contain any sample, to reduce differences in detector sensitivity. The average intensity and standard deviation of each pixel's rocking curve determined and used in grey-scale image as a means of reducing the dimensionality of the data. The data were ordered into a three dimensional array, with the 'x' and 'y' dimensions corresponding to the spatial coordinates of the image and 'z' direction corresponding to the rocking curve angle, i.e. each of the 11, 21 or 31 points in the z direction represented by a different angle on the rocking curve. The samples were imaged in both Sy-DEI planar and Sy-DEI-CT mode. The variability of the background noise is assed, from the difference between the signal and background noise divided by the standard deviation of the signal from the background. The generic term "Signal-to-noise ratio", is measure of true signal to noise (SNR). It is the square root of the number of the averages and phase steps and closely related to the acquisition time (SNR = μ/σ, where 'σ' is the standard deviation and 'μ' is mean of the given data).

Seeds and the developed seeds were placed in plastic container and fixed at the center of the container. The seed was fixed carefully on the sample stage of the system, because the CT reconstruction was susceptible to a sample drift during the data collection. The laterals and the subsequent laterals are fixed in a hollow cylinder of 5 mm inner diameter with a 2 mm wall thickness, to avoid any artifacts, when the sample rotates. A silicon (333) analyzer crystal was placed after the sample stage and rotating using 1 μrad steps to capture only those photons striking it at the correct Bragg angle. Separated by 1 μrad steps, 11, 21, or 31 images were captured in addition to a background image which was made with the beam shutter closed. Photons reflected from the analyzer crystal were captured using a Fuji HR-V image plate with a Fuji BAS-2500 reader, taking approximately 30 s to record each image. ImageJ/Fiji software was used to process and visualization of the images and image analysis.

3 Results

Sy-DEI, images acquired in planar mode are shown in fig's. 5 (a) to (c). Statistical analysis of the marked areas is also shown, for each figure, with standard deviation. The mesh structure of the leaf at the central position is less dense as distinguished from the extreme ends. The embedded root architecture can be observed in the image, since the sample refracts X-rays to a greater extent than the surrounding matrix. Darker pixels in the attenuation image indicate regions where greater refraction or scatter occurred. DEI images of the plant with leaf, growth, root architecture in the marked areas of the leaf, in planar mode with profile nature, are shown in Fig. 6 for comparison of the image with different analyzer settings. The growing seed is denser than parts of the seed architecture and thus caused significant x-ray refraction. Further analysis of the data could provide useful information about the amount of the refraction and scatter resulting at each pixel, which could then be interpreted as relative density and concentration of ordered molecules, respectively.

The physiology and the associated morphology of sample is useful for determining the structure and enhancement of some desired property, for example, soft external layer and interior soft structure. It will be possible to differentiate the weak and strong attenuation in the sample. The soft external layer has soft part inside with two hallow parts for the development of the plant and the associated physiology. This way, we may be able to differentiate weak and strong attenuation in the sample, to know more about the contrast mechanisms.

We have chosen the beam profile, projection area, are at the peak position of the rocking curve of the sample. The intensity profile is symmetric, towards the low-angle, high-angle and at the peak position.

For planar imaging, we acquired 21 images at different analyzer positions of the sample. Figure 7 (a) to (c) shows, Sy-DEI-CT refraction images of the sample, towards the low angle side, high-angle side, and at the peak position. The brighter area in the images represents the low X-ray intensity or more apparent absorption. The analyzer crystal is tuned to the peak of the rocking curve to create contrast due to the rejection of ultra-small-angle X-ray scattering (USAXS). This way, we characterized the extinction contrast of the plant in Sy-DEI-CT mode. The peak image of Fig. 7(c) shows, significant extinction contrast. The images show the effectiveness of the tomography mode for better visualization. Sy-DEI-CT mode relies on the phase contrast between the sample and the surrounding medium, to image the transparent structures, such as, soft part of the outer layer and the embedded inside protein, which in turn due to refractive index differences. It is interesting to note that, in the energy region from 15 to 30 keV, the phase shift term 'δ' is of the order of 10^{-7} and the absorption term 'β' is of the order of 10^{-10}, reflecting to reveal the phase effects even if the absorption contrast is low. The contrast has considerable visibility in the tomographic mode. The reconstructed image of the root architecture, has a nature of porosity, with a wide hallows nature. The problem with tomography is that a large number of images must be captured, resulting in greater radiation exposure. Radiation exposure with two-dimensional DEI is low. The effects of radiation damage can be reduced by reducing exposure times and frequencies or by reducing the number of data points included in the rocking curve.

4 Discussion

Compared the reconstructed root images from ((Fig. 7 (a) to (c)) with planar images from (Fig. 5(a) to (c)). It is obvious that the number of laterals and the subsequent laterals have same dimensions of roots and the associated morphology of the plant growth. Furthermore, fine roots with diameters less than 0.5 mm are detected and all artefacts from the background and sample container are removed. This is of great importance for a consecutive analysis mapping the laterals and the subsequent laterals of the root architecture system at 9 μm resolution. Internal root architecture of the sample, with and without filter and intensity profile in DEI-CT mode is shown in Fig. 7 (a) to (c). These images were obtained, after directly thresholding the filtered data. The same threshold level is applied to other images. Figure 8 (a) to (c), shows the interior variation of the intensity of the sample at the spatial coordinates of X and Y with

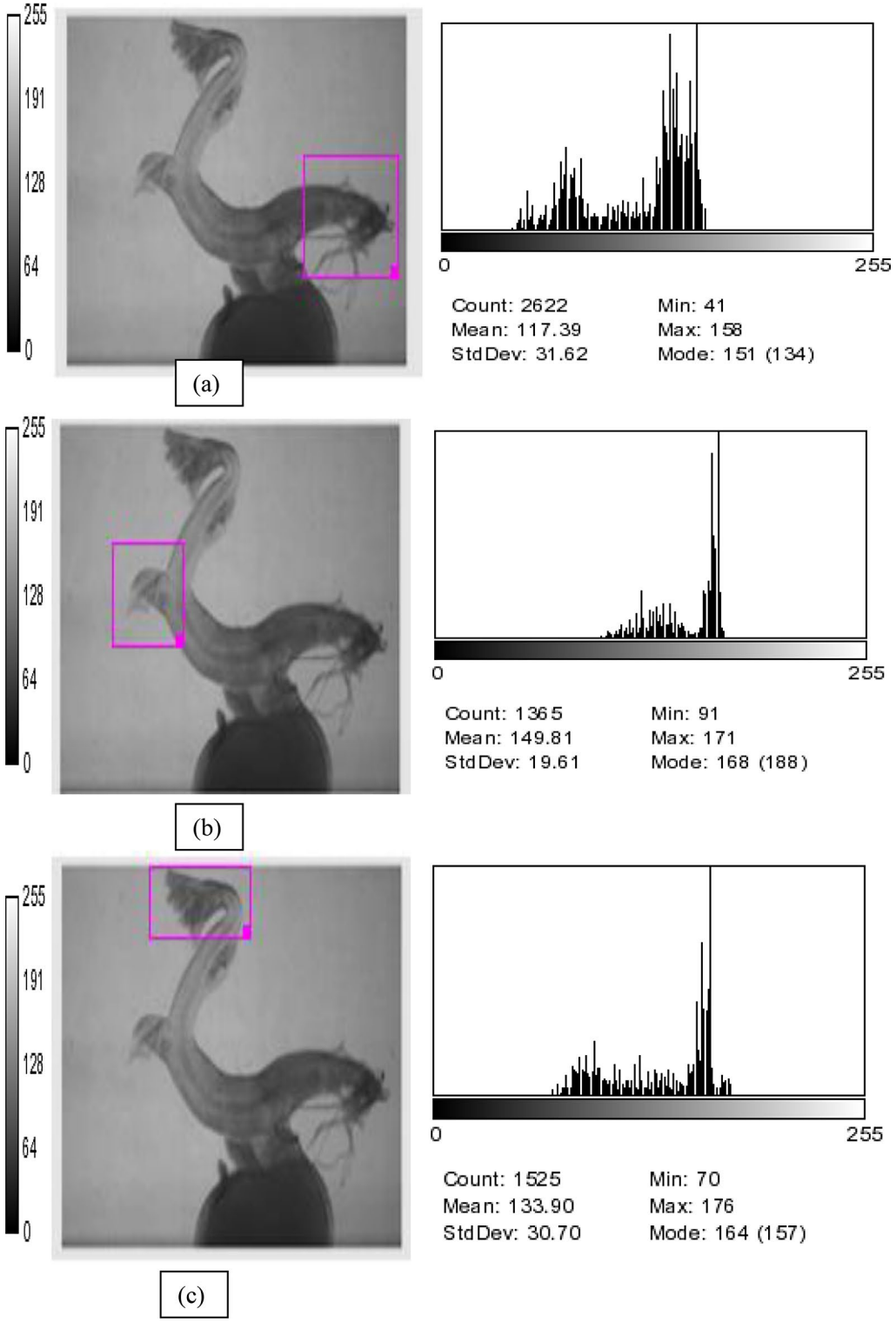

Fig. 5 (**a**) to (**c**). DEI images of the plant with leafs, growth, root architecture in the marked areas of the leafs, in planar mode. Marked areas are used for image analysis in DEI-CT mode. Inside boxes are considered regions of interest of intensity variations, at three different positions and the associated histograms

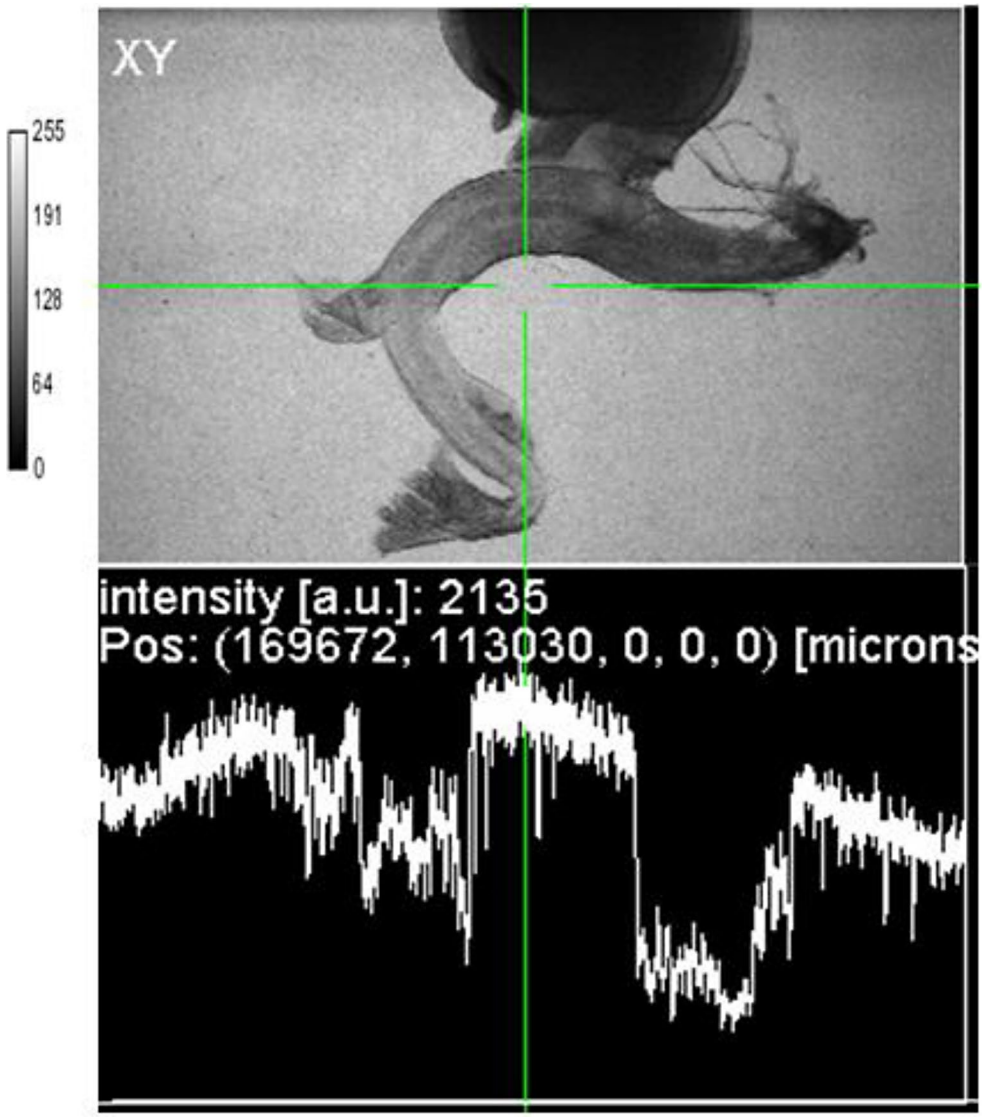

Fig. 6 DEI image of the plant with leafs, growth, root architecture in the marked areas of the leafs, in planar mode with profile nature

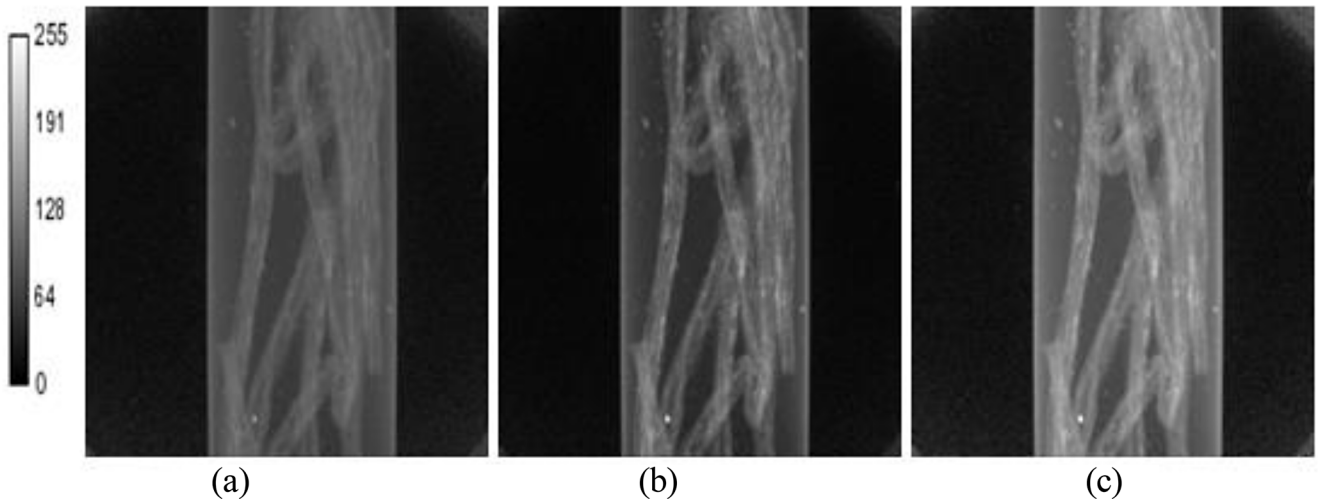

Fig. 7 Internal root architecture structure of the sample in DEI-CT mode. Filtered CT images (**a**) Image at low- angle side of the root (**b**) Image at high-angle side of the root (**c**) Image at the peak position of the rocking curve

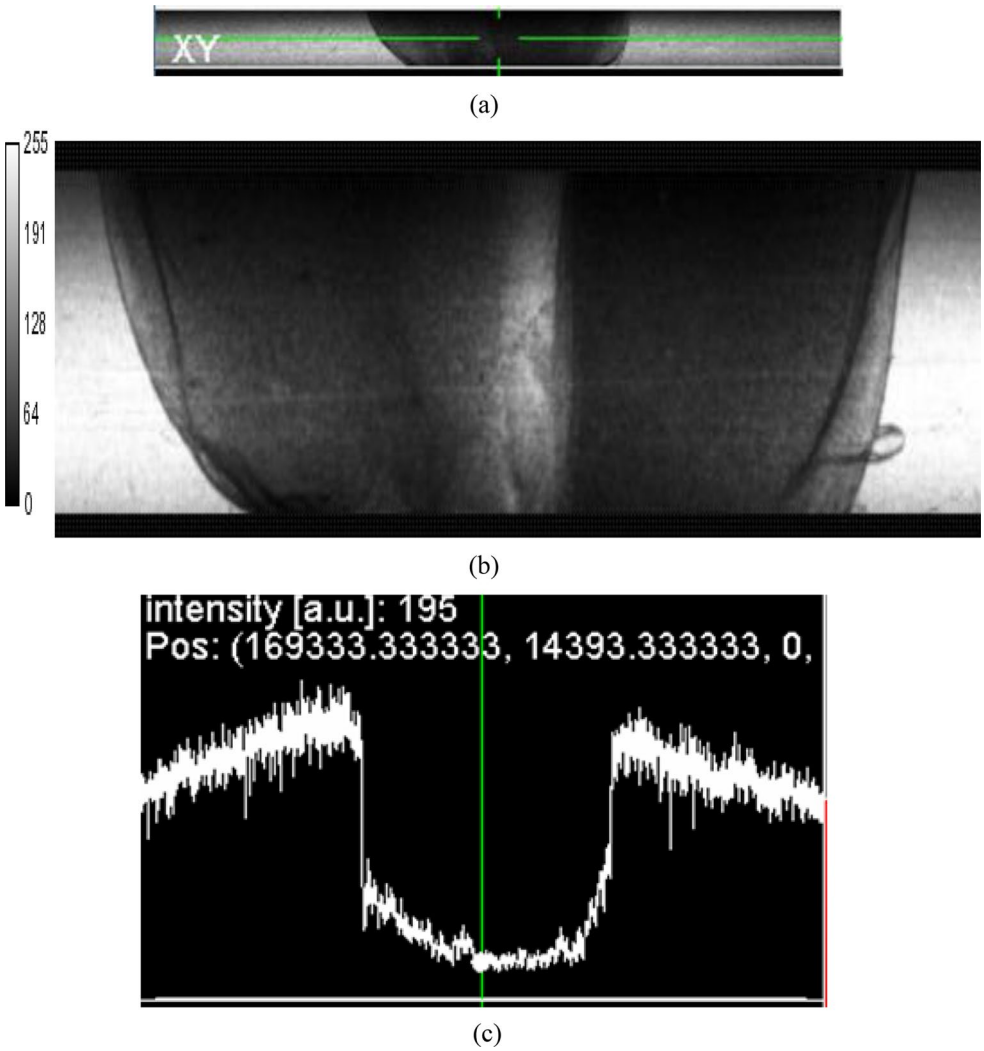

Fig. 8 (**a**) to (**c**). Interior variation of the intensity of the sample at the spatial coordinates of X and Y. (**a**) DEI-CT 2D image (**b**) DEI-CT 2D filtered image (**c**) Intensity profile of the image

enhanced contrast, at the beginning of the seed growth and profile at the center position of the seed. Figure 9 shows, the DEI image of the seed growth in the planar mode. Figure 10 shows, DEI image of the seed in the planar mode at central position of the sample. Figure 11 shows, the DEI-CT image of the seed growth visible with 3D viewer, with acceptable contrast. Figure 12 shows, the image of the interior root architecture of the sample with DEI - CT system, with enhanced contrast at the bottom of the sample, at the laterals and the subsequent laterals of the sample. Prepared the filtered sinogram at the top, bottom, center positions and ROI. Inset shows (Fig. 12) the sinogram, with 10 images in ROI. From the filtered sinogram, tomographic images were reconstructed. Contrast enhancement, from DEI-CT slices for three different treatments are displayed. Figure 13 shows, the interior root architecture of the sample with DEI-CT system with enhanced contrast around the soft part of the sample, when the growth rate starts, at the laterals and the subsequent laterals of the sample, with clear visibility of the channel as shown in Fig. 4 around the ROI. Different components of the sample are more distinguishable; to reflect the interior structure, allowing the internal features of the sample. Figure 14 (a) to (b) shows, the z-projection of a DEI-CT refraction data image slice of a dry seed, visualized at low-resolution observation (high-resolution) and an overall morphological development of seeds during the germination process. The z-projection of the standard deviation through several DEI-CT slices allowed for easy mapping of the internal embedded features. Internal features with void space for a low water content of a dry seed after 24 h;

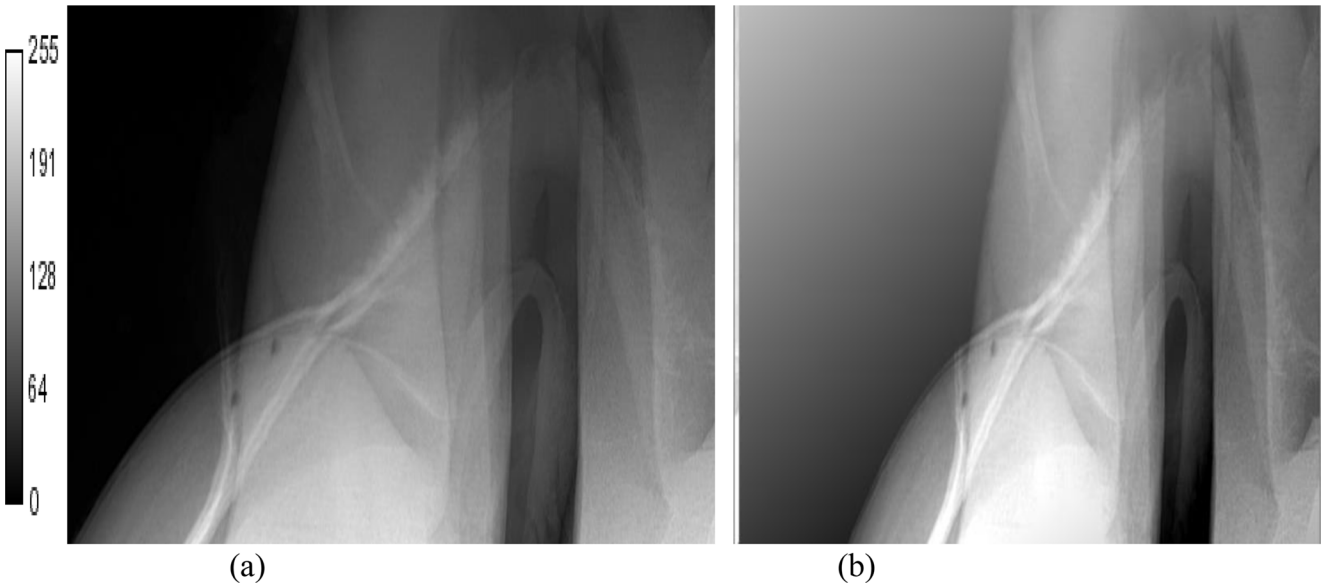

Fig. 9 DEI image of the seed growth in the planar mode (**a**) without filter (**b**) with Gaussian filter

Fig. 10 DEI-CT image of the seed at central position of the sample

reflects the importance of the dryness for better contrast in the CT image. 3D data set provided higher field of view for the sample. DEI-CT images are sharper with 30 keV X-rays and refracted X-rays are measured as data. X-rays refract at density interfaces, regardless of the energy of the incident photons, at outer layer and soft part of the sample. An additional advantage of using high-energy X-rays is that the absorbed radiation dose is low. The amount of radiation absorption has been calculated to be < 1% and approximately 0.12 mGy per exposure. The radiation dose was calculated for the 2D scan in planar mode and for CT, high radiation dose due to higher exposures. In both cases, it differs less < 1%. This amount of exposure is not expected to affect germination or growth significantly. The visibility of the seed channel is clearly seen, when the seed growth starts at the bottom. The seed growth reflects on denser parts of the seed and thus caused significant X-ray refraction. Diffraction-enhanced imaging between the samples and surrounding medium to image transparent structures, which in turn due to refractive index differences, arising from leafs and subsequent leafs.

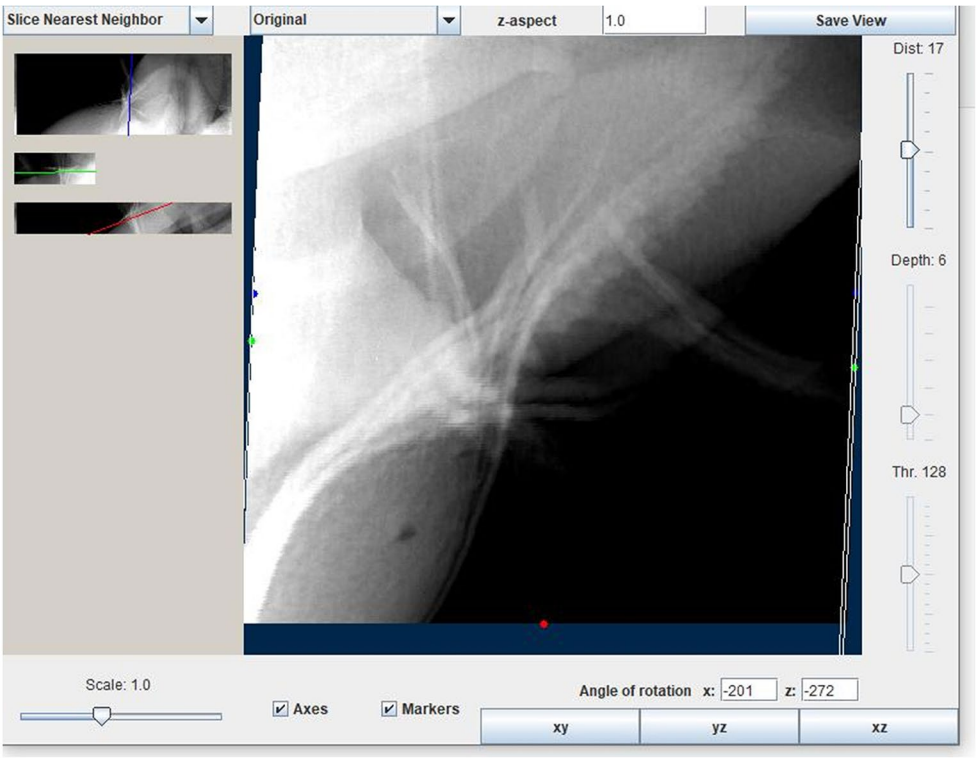

Fig. 11 DEI-CT image of the seed growth visible with 3D viewer plugin

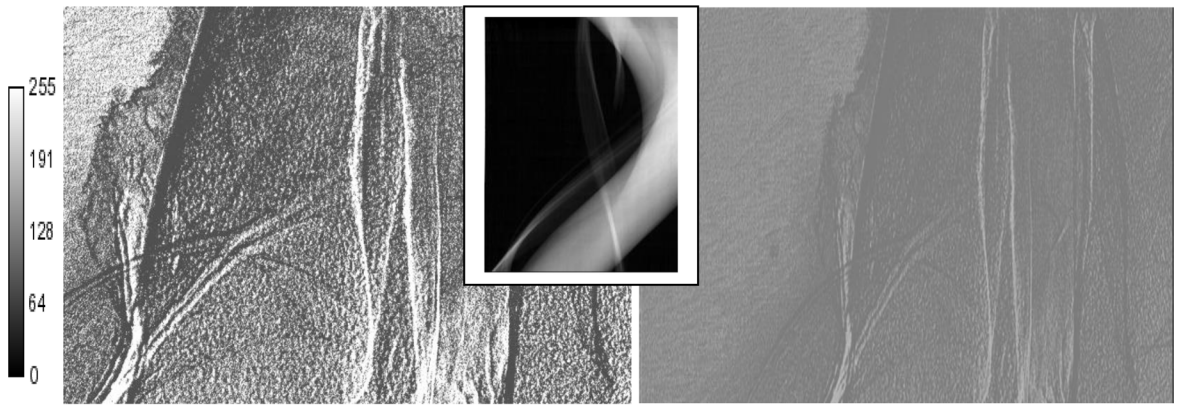

(a) (b)

Fig. 12 DEI-CT slice image of the interior root architecture of the sample. Images acquired at the half-reflectivity point (6.5 µrads) for 30 keV 111 reflection (**a**) Enhanced contrast at the bottom of the sample (**b**) Enhanced contrast at the laterals and the subsequent laterals of the sample. Inset shows the sinogram, with 10 samples from ROI

These systems and the associated software, allowed us, successfully, to reconstruct the fine root architecture of the laterals and subsequent laterals in Sy-DEI-CT. For the present image analysis and the scanning resolution of the Sy-DEI-CT system, it will be possible to observe and detect processes of the fine root architecture of laterals and the subsequent laterals, which are essential for plant growth. With the development of new digital technology, algorithms, it will be easy to visualize the interior root architecture of the laterals and the subsequent laterals, with more visibility.

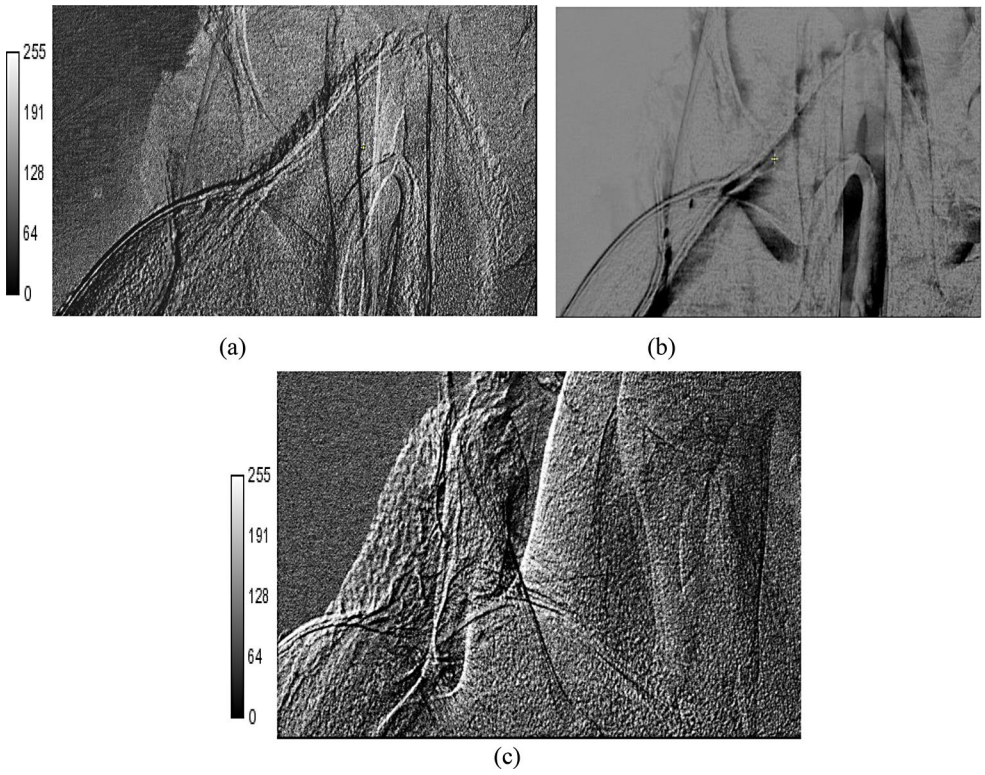

Fig. 13 DEI-CT slice image of the interior root architecture of the sample. Images acquired at the half-reflectivity point (6.5 μrads) for 30 keV 111 reflection (**a**) Enhanced contrast around the soft part growth of the sample (**b**) Enhanced contrast at the laterals and the subsequent laterals of the sample, with clear visibility of the channel as shown in Fig. 4 with 10 samples from ROI (**c**) Enhanced contrast at the central position of the sample as shown in Fig. 8(**a**) to (**c**)

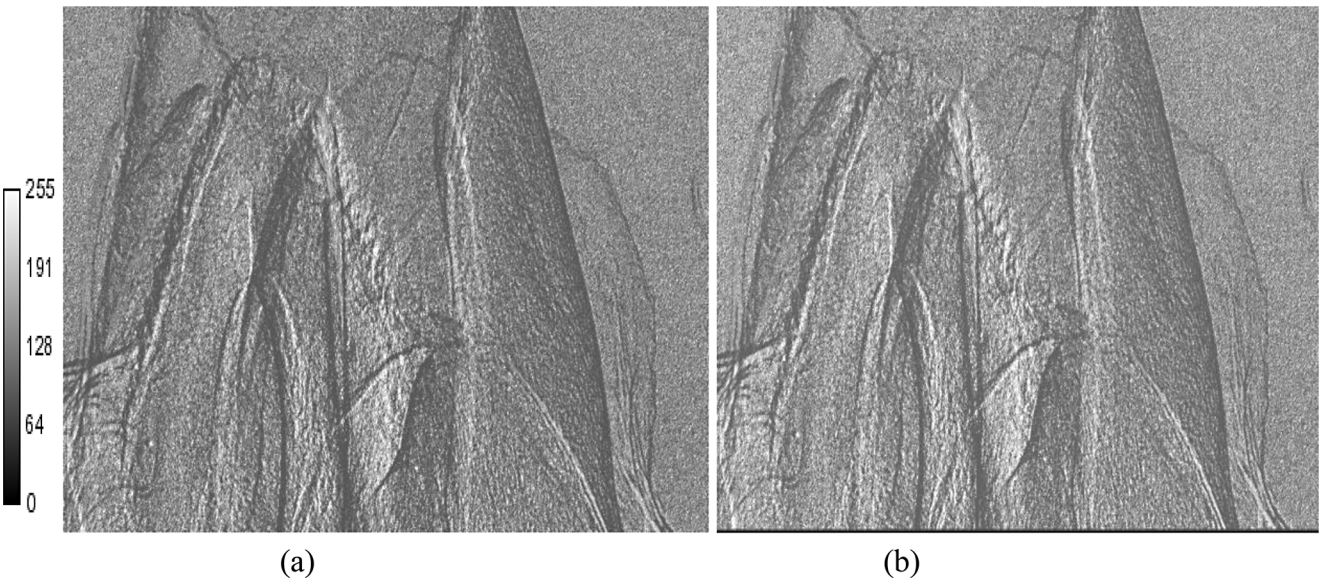

Fig. 14 Z-projection of a DEI-CT refraction data set slice image of a dry seed with low water content (**a**) Low-resolution (**b**) High-resolution. Low and high contrast between soil pore space and roots

5 Conclusions

Root architecture of the plant grown from seeds provides new information about the structure and enhancement of some desired property, for example, interior micro-structure of the root laterals and the subsequent laterals and the clear visibility of the leaves in detail, in planar mode, in marked areas. This way, it will be possible to differentiate the weak and strong attenuation of the signal traversing within the sample, clearly reflecting the acceptable visibility, defined by the detector resolution in CT mode, in root laterals, subsequent laterals and the associated opaque matrix with enhanced contrast. The sample has a thin layer of soft structure outside and protein inside. The visibility, contrast and porosity, with finer details, can be noticed, with Sy-DEI-CT

systems as distinguished from Sy-DEI. However, limited field of view, may limit the problems associated with Sy-DEI-CT. Further, these techniques have challenges such as low contrast between soil pore space and roots, long X-ray imaging time, and low spatial resolution.

Acknowledgements One of the author's (DVR) undertook part of this work as visiting professor with a financial support from, Department of Science Based Applications to Engineering, Universita di Roma La Sapienza", Via Scarpa 10, 00161, Roma, Italy, Istituto di Matematica e Fisica, Universita di Sassari, Italy, ICTP, Trieste, Italy and Department of Bio-Systems Engineering, Yamagata University, Yonezawa, Japan "Use of the National Synchrotron Light Source, Brookhaven National Laboratory, was supported by the U.S. Department of Energy, Office of Science, Office of Basic Energy Sciences, under Contract No. DE-AC02-98CH10886".

Data availability Data will be made available on request.

Declarations

Additional Information The potential author (D.V.Rao) collaborated with G.E.Gigante, Science Based Applications to Engineering, Universita di Roma " La Sapienza", Rome, Italy.

Competing interests The authors declare that they have no known competing financial interests or personal relationships that could have appeared to influence the work reported in this paper.

References

1. L. Brombal, F. Arfelli, F. Brun, V.D. Trapani, M. Endrizzi, R.H. Menk, P. Perion, L. Rigon1, M. Saccomano, G.Tromba and, A. Olivo, Phys. Med. Biol. **69**, 075027 (2024)
2. A. Astolfo, I.G. Haig, D. Bate, A. Olivo, P. Modregger, Phys. Scr. **98**, 095501 (2023)
3. L. Brombal, F. Arfelli, R.H. Menk, L. Rigon, F. Brun, Sci. Rep. **13**, 4206 (2023)
4. L. Quenot, S. Bohic, E. Brun, Appl. Sci. **12**, 9539 (2022)
5. L. Brombal, L. Rigon, F. Arfelli, R.H. Menk, F. Brun, J. Instrum. **17**, C01043 (2022)
6. D. Legland, C. Alvarado, E. Badel, F. Guillon, A. King, T.D. Quoc Le, C. Rivard, L. Paré, A.-L. Chateigner-Boutin, C. Girousse, Appl. Sci. **12**, 3454 (2022)
7. S. Tao, C. He, X. Hao, C. Kuang, X. Liu, Appl. Sci. **11**, 2971 (2021)
8. M. Endrizzi, Nucl. Instrum. Methods Phys. Res. A **878**, 88 (2018)
9. N. Kunishima, Y. Takeda, R. Hirose, D. Kalasová, J. Šalplachta, K. Omote, Plant. Methods. **16**, 7 (2020)
10. D. Chapman, W. Thomlinson, R.E. Johnston, D. Washburn, E. Pisano, N. Gmu¨r, Z. Zhong, R. Menk, F. Arfelli, D. Sayers, Phys. Med. Biol. **42**, 2015 (1997)
11. Z. Zhong, W. Thomlinson, D. Chapman, D. Sayers, NIM A **450**, 556 (2000)
12. O.G.Duliu, Earth Sci. Rev. **48**, 265 (1999)
13. P.J. Gregory, D.J. Hutchison, D.B. Read, P.M. Jenneson, W.B. Gilboy, E.J. Morton, Plant. Soil. **255**, 351 (2003)
14. M.A. Hamza, S.H. Anderson, L.A.G. Aylmore, Aust. J. Soil Res. **39**, 1387 (2001)
15. D.A. Heeraman, J.W. Hopmans, V. Clausnitzer, Plant. Soil. **189**, 167 (1997)
16. J.S. MacFall, G.A.Johnson, *Special Publication No. 36* (Soil Science Society of America, Madison, USA, 1994), p. 99
17. J.S. MacFall, M.W. Jennette, T.W. Rufty, Crop Science Society of America and Soil Science Society of America, Charlotte, North Carolina, (2001), 24 October 2001
18. C.J. Moran, A.P.A.W. Stevenson, Plant. Soil. **223**, 99 (2000)
19. J.S. Pierret, S.O. Prasher, A. Kantzas, C Langford Soil. Sci. Soc. Am. J. **63**, 1530 (1999)
20. A.Pierret, Y.Capowiez, C.Moran, A.Kretzschmar, Geoderma **90**, 307 (1999)
21. C.J. A.Pierret, J.M. McLachlan, Image Anal. Stereology. **19**, 145 (2000)
22. A.Pierret, M.Kirby, C.Moran, Plant. Soil. **255**, 361 (2003)
23. K.W.T.M.S.T.F.A.B.K. Huang, Nondestructive root-zone analysis with X-ray CT scanner, Paper 923018. (1992), Society of Agricultural Engineers, St.-Joseph, MI, USA, p. 15
24. J.R. D.Wulfsohn, Plant. Soil. **214**, 15 (1999)
25. H.M. Taylor, D.R. Upchurch, J.M. Brown, H.H. Rogers, Some methods of root investigations, in *Plant Roots and Their Environment*, ed. by B.L. McMichael, H.Persson, (Elsevier Science, Amsterdam, Netherlands, 1991)
26. A. Timmerman, J.F. Delerue, S.Herman, J.Feyen, Determination of hydraulic parameters and X- ray quantification of 3D porous structures. 17th World Congress of Soil Science. Paper 1391, Thailand, (2002),14–21 August, p. 12
27. R. Zwiggelaar, C.R. Bull, M.J. Mooney, J. Agric. Eng. Res. **63**, 161 (1996)
28. D.V.R.R.C.A.B.Z.Z.T.A.T.Y.G.E. Gigante, J. Food Meas. Charact. Food Measure. **7**, 13 (2013)
29. L.W. Young, C. Parham, Z. Zhong, D. Chapman, M.J.T. Reaney, J. Exp. Bot. **58**(10), 2513 (2007)
30. T. Kao, C.L.X.Y.X.L.Y.D. Connor, A. Dilmanian, C.Parham, M. Reaney, Z.Zhong, Nucl. Instrum. Meth A 582, 208 (2007)
31. L. Li, Q. Zhang, D. Huang, Sensors. **14**, 20078 (2014)
32. D. Leister, D.C. Varotto, P. Pesaresi, A. Niwergall, F Salamini Plant. Physiol. Biochem. **37**, 671 (1999)
33. M.M.D. Truhn, K. Nagel, A. Walter, H. Scharr, T.A. Heidelberg, Germany, (2008),497–506
34. E.W. Tollner, E.L. Ramseur, Techniques and approaches for documenting plant root development with X-ray computed tomography, in *Tomography of Soil–Water–Root Processes. Special Publication No. 36*, ed. by S.H. Anderson, J.W. Hopmans (Soil Science Society of America, Madison, USA, 1994), p. 115
35. A.P.X. Sirauly, S. Berry, R Furbank J. Fripp BMC Plant. Biol. **12**, 63 (2012)
36. T.Grift, J.Novais, M.Bohn, Biosyst Eng. **110**,40 (2011)
37. W.H. Stuppy, J.A. Maisano, M.W. Colbert, P.J. Rudall, T B Rowe Trends Plant. Sci. **8**, 2 (2003)
38. C.E. Hargreaves, P.J. Gregory, A.G. Bengough, Plant. Soil. **316**, 285 (2009)
39. M. Lontoc-Roy, P.D.S.O. Prasher, L. Han, T.Brouillet, D.L.Smith, Geoderma 137, 231 (2006)
40. J.S.P.M. Al-Belushi, M Deadman Soil. Biol. Biochem. **39**, 391 (2007)
41. S.R. Tracy, J.A. Roberts, C.R. Black, McNeill R Davidson S J. Mooney, J. Exp. Bot. **61**, 311 (2010)
42. Z. Zhong, W. Thomlinson, D. Chapman, D. Sayers, Nucl. Instrum. Methods a **450**, 556 (2000)
43. Z. Zhong, D. Chapman, D. Connor, A. Dilmanian, N. Gmur, M. Hasnah, R. Johnston, M. Kiss, J. Li, Synchrotron Radiat. News. **15**, 27 (2002)

44. D.V. Rao, M. Swapna, R. Cesareo, A. Brunetti, Z. Zhong, T. Akatsuka, T. Yuasa, T. Takeda, G.E. Gigante, Appl. Radiat. Isot. **68**, 1687 (2010)